Transparent Conducting p-type NiO:Li thin films prepared by Spray Pyrolysis Technique

[1]S. Mani Menaka, [2]G. Umadevi
[1]Research Scholar, [2]Associate Professor
[1]Research and Development Centre,
[1]Bharathiar University, Coimbatore - 641046, Tamilnadu, India
[2]Dept. of Physics, Govt. Arts College, Coimbatore - 641018, Tamilnadu

Abstract: Pure nickel oxide (NiO) and lithium-doped nickel oxide (NiO:Li) thin films are deposited on glass substrates by the spray pyrolysis technique using nickel chloride hexahydrate and lithium chloride monohydrate as starting materials. The effects of lithium concentration (0-8%) on the XRD, SEM, FTIR, UV-Vis-NIR, and electrical analysis of the films are studied. XRD structural analysis showed that all the NiO and NiO:Li films exhibit polycrystalline cubic structure with (200) preferred orientation. XRD results showed that the crystallite sizes are around 17.86 nm to 21.43 nm. The optical band gap decreases from 3.94 eV to 3.69 eV. All the NiO and NiO:Li films are p-type. The carrier concentration of 3.98×10^{16} cm^{-3}, carrier mobility of 2.76 cm2 V^{-1} s^{-1}, and low resistivity of 0.56×10^{2} Ω cm are reasonable values for p-type TCO thin films.

***IndexTerms* - Nickel oxide; Thin films; Spray pyrolysis; Grain size; Band gap; Resistivity**

I. INTRODUCTION

In contrast to n-type Transparent conductive oxide (TCO) thin films like SnO_2, In_2O_3, and ZnO, the NiO shows p-type semiconductivity. Indeed not many oxides are easily p-type. Usually the p-type conductivity is due to the metal deficit or O_2 excess. Due to the wide band gap energy from 3.6 to 4 eV [1,2], NiO has a wide range of applications in optoelectronic devices. NiO thin films can be prepared by various chemical and physical methods, such as chemical vapor deposition [3], pulsed laser deposition [4], electrochemical deposition [5], e-beam evaporation [6], vacuum evaporation [7], magnetron sputtering [8], sol–gel [9], and spray pyrolysis [10].

Among the methods, the spray pyrolysis (SP) technique is a very easy, low cost, safe, cheap, non-vacuum system of deposition method, particularly useful for large area applications.

Spray pyrolysis has been employed in the past to deposit NiO films through metal salts such as nitrates, acetates and sulphates. Aqueous solutions are commonly used in SP system to deposit thin films due to the availability of a wide range of water-soluble metal salts. Metal chlorides have highest water solubility relative to other metal salts and are used for the industrial production of several oxides and ferrites. In our study, nickel oxide particles were prepared by spray pyrolysis of aqueous solution of $NiCl_2\cdot6H_2O$.

Due to its high chemical stability, as well as optical, magnetic and electrical properties, NiO has a wide range of applications such as light emitting diodes [11], liquid crystal displays [12], n-p junction electrodes in dye sensitized solar cells [13], solar cells [14], solar filters [15], fuel cells [16], photo electrolysis [17], p-type transparent film [18], anti-ferromagnetic material [19], chemical sensors [20], electronic devices [21], and electrochromic devices [22].

To investigate the effects of Li concentration on Li doped NiO films, the XRD, SEM, FTIR, UV-Vis-NIR, and electrical analysis of the films are studied. Pure stoichiometric NiO exhibits high electrical resistivity at room temperature. The p-type conductivity on NiO can be significantly increased by doping with monovalent Li ions [23]. The main aim of this study was to reduce the electrical resistivity of films and to study the effect of Li concentration on the properties of films to develop the possible application of these materials.

II. EXPERIMENTAL

2.1 Film Synthesis

Pure and NiO:Li thin films were prepared using nickel chloride hexahydrate ($NiCl_2\cdot6H_2O$) and lithium chloride monohydrate ($LiCl.H_2O$) as the starting materials. The isopropyl alcohol was added in a solution to reduce the surface tension on glass substrate. The films were deposited onto glass substrates using the spray pyrolysis technique which were chemically and ultrasonically cleaned before deposition. During the film deposition the substrate temperature was kept constant at 450 ºC. This temperature was found to be optimum to obtain good adherent pure NiO and NiO:Li films. For deposition of pure films, 0.1 M of $NiCl_2\cdot6H_2O$ was dissolved in distilled water to make precursor solution. For deposition of doped films, the precursor solution was prepared by dissolving $NiCl_2\cdot6H_2O$ and different concentrations (2%, 4% and 8%) of $LiCl.H_2O$ in distilled water. The optimized conditions were arrived at the following parameters: spraying time (5 sec), spray interval (2 min), deposition rate (8 ml/min), pressure of the carrier gas (1.5 bar) and spray nozzle-substrate distance (30 cm) were kept constant for each concentration.

2.2. Film Characterization

A 'Rigaku' X-ray diffractometer (XRD) with a CuKα radiation (λ=1.5418Ǻ) was used for structural studies in the range of 2θ = 10–90°. The surface morphology of the films was observed by a 'JSM 35 CF JEOL' model Scanning electron microscopy

(SEM). The infrared spectra of the as-deposited films were recorded using a 'Shimadzu' Fourier transformed infrared spectroscopy (FTIR) in the range of 400–3800 cm^{-1}. The optical absorbance spectra of the films was taken from a 'Perkin Elmer Lambda' UV-Vis-NIR spectrophotometer in the range of 200–2400 cm^{-1}, and then the optical band gap of the films were calculated using the optical method. The majority carrier types of the as-deposited films were carried out by the Hot probe technique and Hall effect system. The electrical resistivities of the films were measured by the 'Ecopia HMS 5000' Hall effect measurement system.

III. RESULTS AND DISCUSSION

3.1 XRD Analysis

Fig.1 shows X-ray diffraction patterns of pure NiO (0.1 M) and NiO:Li thin films with various (2%, 4%, 8%) lithium doping concentrations. The pure NiO and NiO:Li films in the range between 10° and 90° were analyzed by XRD technique to study the structural identification and changes in the crystalline. Only peaks corresponding the (111), (200), (220) and (222) directions are visible and all the peaks visible belong to the cubic NiO phase (JCPDS 04-0835). The positions of the peaks and the presence of more than one diffraction peak lead to the conclusion that the films are polycrystalline in nature with a cubic crystalline structure. Both the pure NiO and NiO:Li films showed a strong reflection along (200) plane, medium reflection along (111) plane and a weak reflection along (220) and (222) planes. The intensity of the planes (111) and (200) increases as the Li concentration increases from 0% to 8%. It is well known that the (200) plane of ionic rock salt materials is considered as a non-polar cleavage plane and is thermodynamically stable. In contrast, the (111) plane is polar and unstable. Therefore, the (200) preferred orientation of NiO:Li films can take on the better conductive properties.

In the pure NiO and NiO:Li, the lattice parameter (a) can be evaluated from the relation [24]:

$$a = d_{hkl}\sqrt{h^2 + k^2 + l^2} \tag{1}$$

where d_{hkl} is the inter-plane spacing, and h, k & l are the indices of the planes.

The inter-plane spacing (d_{hkl}) can be calculated using the Bragg law [25] :

$$d_{hkl} = \frac{\lambda}{2\sin\theta} \tag{2}$$

where λ is the X-ray wavelength (0.1548 nm for CuKα), and θ is the diffraction angle.

The grain sizes (D) of the crystallites are calculated for major reflex (200) using the Scherrer's formula [26]:

$$D = \frac{k\lambda}{\beta\cos\theta} \tag{3}$$

where k is the dimensionless number equal to 0.9, λ is the X-ray wavelength, β is the full width at half maximum (FWHM) of diffraction peak and θ is the Bragg diffraction angle.

As the Li concentration increases, a notable change in lattice parameter is not observed. This is due to the slight variation of ionic radius of Li^+ (0.76 Å) compared to that of Ni^{2+} (0.69 Å). The standard value of NiO is 4.170 Å, so the unit cell is not distorted. The average lattice parameter of the pure NiO and NiO:Li films for (200) plane is found to be 4.185 Å, which is very close to the standard value.

In addition, the increase in the intensity of the peaks may be attributed to the grain growth associated with the increase in the crystallite size by increasing the Li concentration. The calculation of crystallite size from XRD is a quantitative approach and is widely used by scientific community. The average crystallite size of the pure NiO and Li:NiO films for (200) plane is 19.12 nm [Table 1].

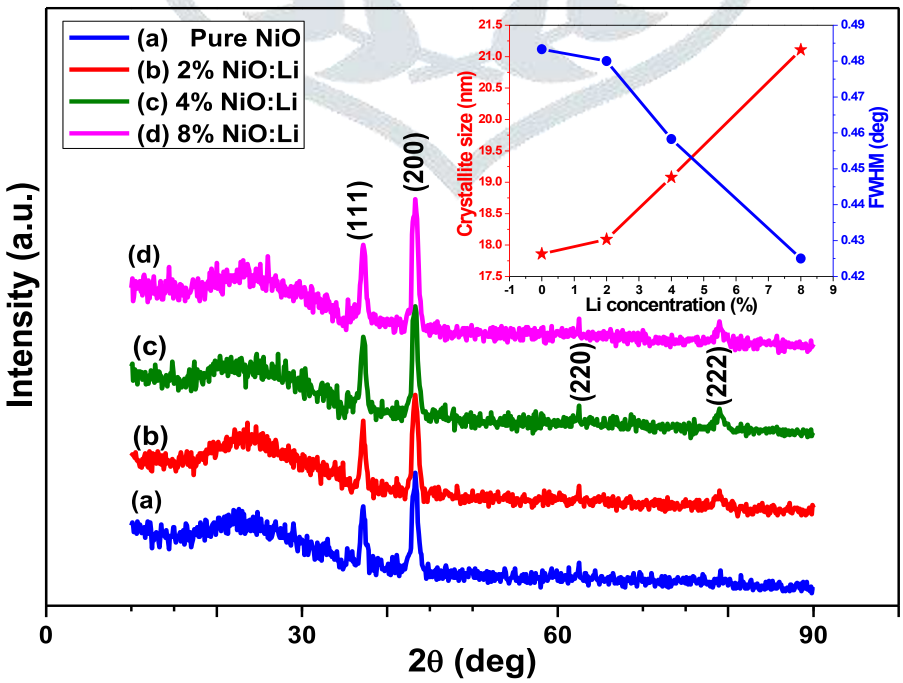

FIG.1: XRD OF PURE NIO AND NIO:LI THIN FILMS

TABLE 1: XRD, UV-Vis-NIR AND ELECTRICAL PARAMETERS FOR PURE NIO AND NIO:LI THIN FILMS

Lithium concen-tration (%)	Crystallite size of XRD (nm)	Band gap (eV)	Resistivity ($\times10^{2}$ Ω cm)	Conductivity ($\times10^{-3}$ Ω^{-1} cm^{-1})	Carrier concen-tration (cm^{-3})	Carrier Mobility (cm^2/V s)
0	17.86	3.94	3.20	3.13	3.38×10^{15}	5.75
2	18.09	3.78	2.50	4.00	5.39×10^{15}	4.62
4	19.08	3.74	1.74	5.75	9.29×10^{15}	3.84
6	-	-	1.08	9.26	1.73×10^{16}	3.30
8	21.43	3.69	0.56	17.86	3.98×10^{16}	2.76

3.2. SEM Analysis

Fig.2 presents high resolution SEM images of pure NiO and NiO:Li thin films with different Li doping concentrations. The SEM images show that the films are formed well and strongly adherent to the substrate. The image of pure NiO shows that the small grains made smooth and best homogeneous thin films with uniform distribution and have a spherical shape. The image of NiO:Li shows that the spherical or circular grains are meet together and agglomerated with each other. The grain size of NiO:Li films increases, and the pores decreases with increase in Li concentration. It is observed that, when the doping concentration is increased, the mobility of the molecules on the surface is improved and causes an increase in grain size.

3.3. FTIR Analysis

FTIR spectroscopy is a non-destructive technique which is associated with functional groups of chemicals. The pellets were prepared by mixing KBr with oxide powder collected by scratching of the film from glass substrate in the ratio 300:1 and then pressing the powder between two pieces of polished steel.

The infrared spectra of the NiO and NiO:Li thin films in the range between 400 and 3800 cm^{-1} were shown in Fig.3. In both the samples, the absorption peak at 451 cm^{-1} is associated to Ni-O vibration bond [27]. In NiO:Li sample, the peak at 973 cm^{-1} is assigned to Li-O vibration bond [28] and the peak at 2020 cm^{-1} is due to the presence of impurities. Observed peak at 1283 cm^{-1} corresponds to the strong C-O stretching vibration, which indicated that the ultrafine powders tend to physically absorbed CO_2 molecule from air. The peaks at 2599, 2868 and 3491 cm^{-1} are due to weak and strong, broad O-H vibration corresponded to the surface absorbed water from atmosphere. The above information confirmed formation of pure and NiO:Li thin films.

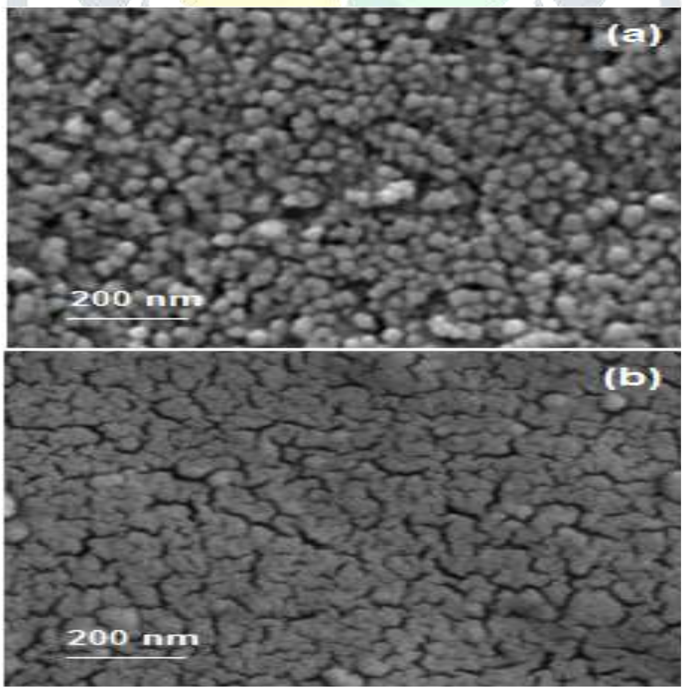

FIG.2. SEM IMAGES OF (A) 0.1 M PURE NIO, (B) 8% NIO:LI THIN FILMS

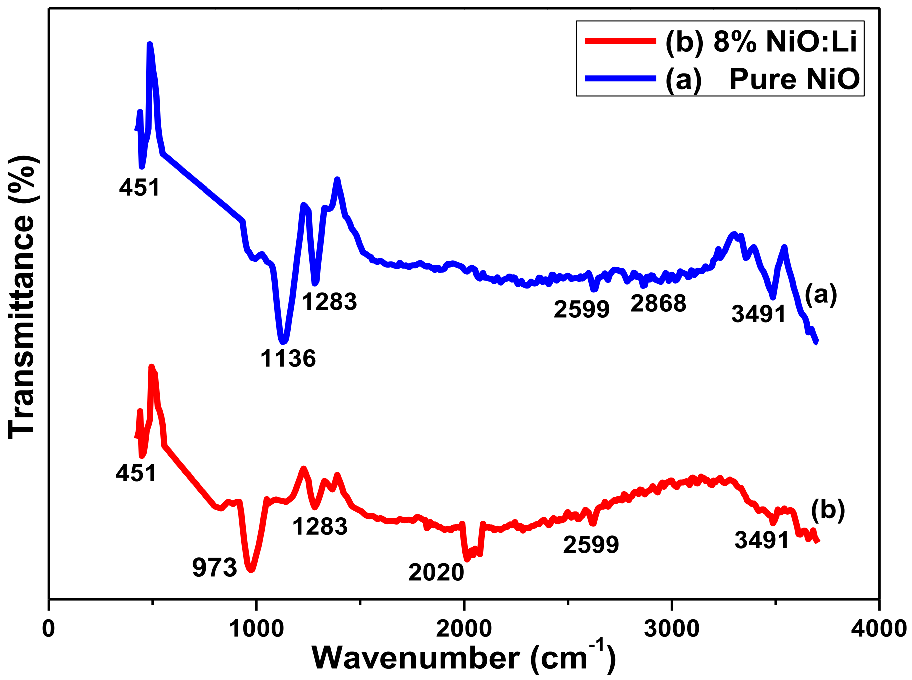

FIG.3. FTIR SPECTRA OF PURE NIO AND NIO:LI THIN FILMS

3.4. UV-Vis-NIR Analysis

3.4.1. Absorption

Fig.4 shows the optical absorption as a function of wavelength in the range of 200-2400 nm for pure NiO and NiO:Li thin films at different concentrations. It is opposite to that of transmittance spectrum. The NiO:Li films show higher absorption in the UV region, and low absorption in the Vis-NIR regions. It has been observed that the absorbance of NiO:Li increases as the Li concentration increases from 0% to 8%. This evident increase of energy is due to the interaction of the material electrons with the incident photons which have enough energy for the occurrence of electron transitions.

3.4.2. Band gap

Fig.5 shows the optical band gap for pure NiO and NiO:Li thin films. The absorption coefficients (α) of the films have been calculated from the optical absorption data using the following relation [29]:

$$\alpha = \frac{2.303\ A}{d} \tag{4}$$

where A is the absorption and d is the film thickness.

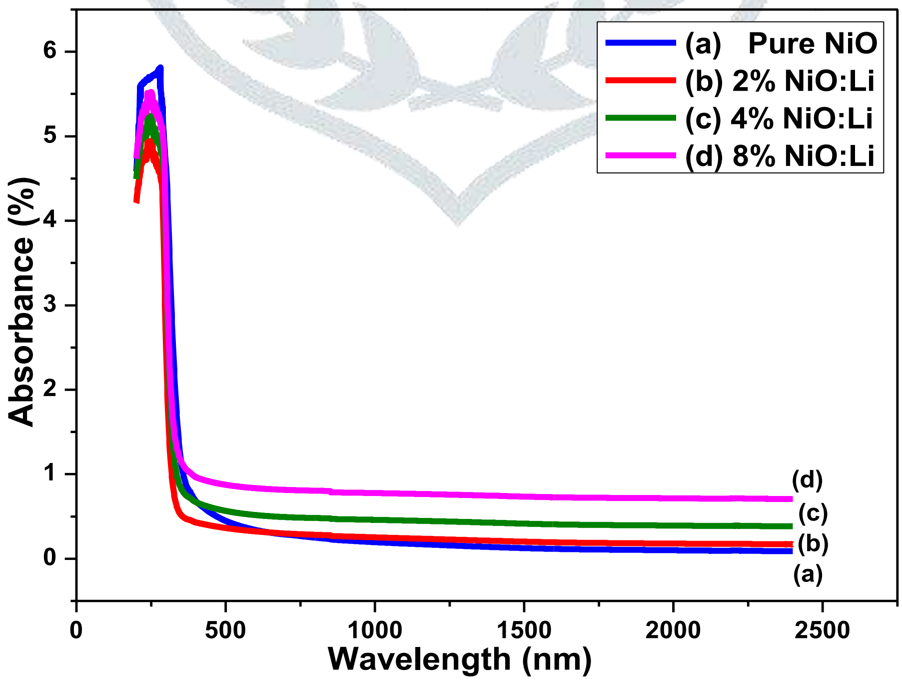

FIG.4. ABSORBANCE VERSUS WAVELENGTH OF PURE NIO AND NIO:LI THIN FILMS

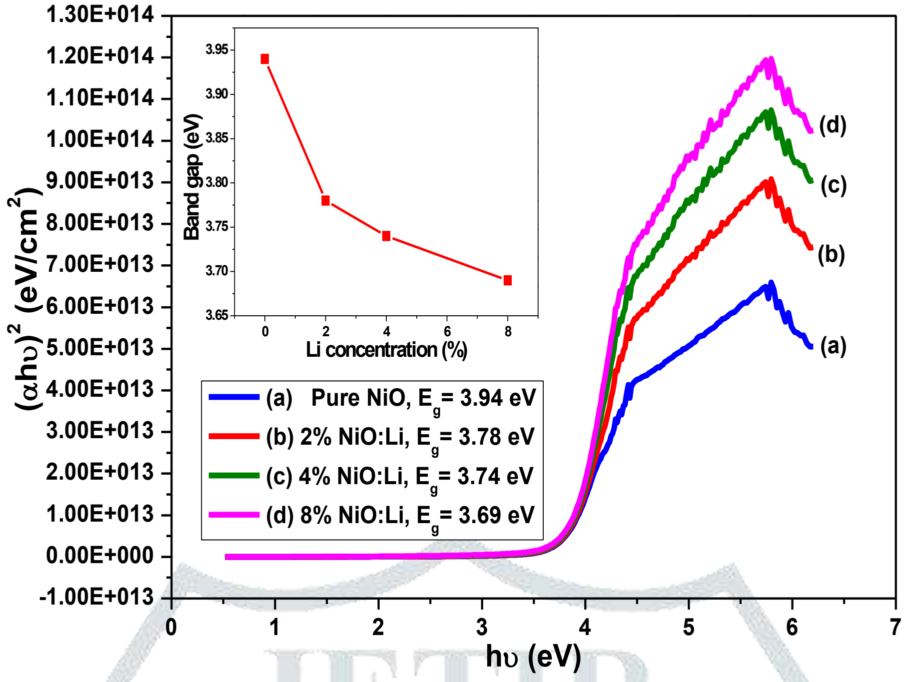

FIG.5. OPTICAL BAND GAP OF PURE NIO AND NIO:LI THIN FILMS

The determination of the optical band gaps of these films have been calculated using Tauc's plot of $(\alpha h\nu)^2$ versus hν and is expressed as follows [30]:

$$\alpha h\nu = A_o (h\nu - E_g)^{n} \tag{5}$$

where α is the absorption coefficient, h is Planck's constant, ν is the frequency of the incident photon, A_o is an energy-independent constant, E_g is the band gap energy, and n is a number equal to 1/2 for direct band gap and 2 for indirect band gap compound.

The band gap energy is determined from the extrapolated straight line portion of the plot to the x axis, $(\alpha h\nu)^2 = 0$. The linear nature of the plots at the absorption edge confirmed that all deposited films pure NiO and NiO:Li films are semiconductor with direct band gap**.** The optical band gap of NiO:Li films gradually decreases from 3.94 eV to 3.69 eV with Li concentration because of the decrease in carrier mobility. These results are caused by the dopant Li ions which act as the scattering center and hinder the carrier to move.

3.5. Electrical Analysis

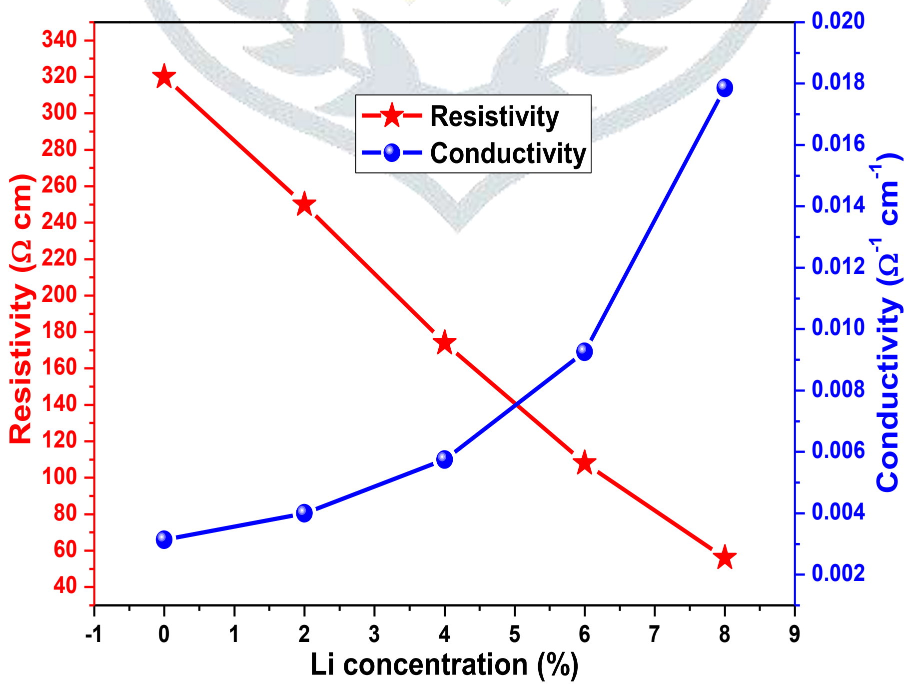

FIG.6. RESISTIVITY AND CONDUCTIVITY OF PURE NIO AND NIO:LI THIN FILMS

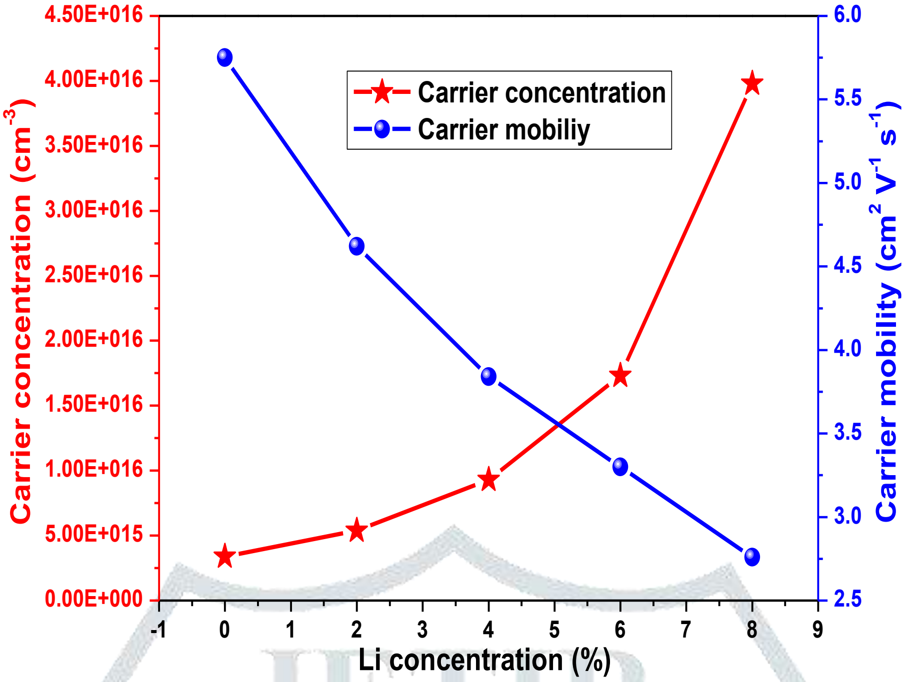

FIG. 7. CARRIER CONCENTRATION AND CARRIER MOBILITY OF PURE NIO AND NIO:LI THIN FILMS

The charge carrier type and the resistivity of the pure NiO and NiO:Li films were measured with the help of Hall System. Hot probe technique confirmed that all the films were p-type. Fig.6 shows the resistivity and conductivity for pure NiO and NiO:Li films with various Li doping concentrations. The resistivity of the pure NiO thin film is 3.20 $\times10^2$ Ω cm. The resistivity decreased substantially to 0.56 $\times10^2$ Ω cm when the Li doping concentration is increased to 8% [Table 1]. As the electrical conductivity is inverse of resistivity, the electrical conductivity increased with Li doping. NiO is a p-type semiconductor due to the Ni^{2+} vacancies. When Li^+ ions (r_{ion}= 0.76 A°) began to substitute for Ni^{2+} (r_{ion}=0.69 A°) ions in normal crystal site positions, each Li^+ is capable of donating only one electron to the O^{2-} and the excess of uncompensated holes increases the p-type behavior of the films, thereby increasing the carrier concentration with a subsequent decrease in the resistivity value in the NiO:Li composite film.

Fig.7 shows the hole carrier concentration and carrier mobility for NiO and NiO:Li films with various Li doping concentrations. The hole carrier concentration of the pure NiO film is 3.38 $\times10^{15}$ cm^{-3}. The hole carrier concentration increased with Li doping, reaching a maximum value of 3.98 $\times10^{16}$ cm^{-3} at a Li concentration of 8%. The carrier mobility decreased from 5.75 cm^2 V^{-1} s^{-1} to 2.76 cm2 V^{-1} s^{-1} with increasing Li content from 0% to 8% [Table 1]. For the carrier mobility, dopant materials as the scattering center, the carrier mobility will encounter more hindered concentration with increasing Li amount, which leads the decrease of mobility.

4. Conclusion

The polycrystalline thin films of pure and NiO:Li are prepared by spray pyrolysis technique onto glass substrate at different concentrations level. The effects of the Li doping concentration on the XRD, SEM, FTIR, UV-Vis-NIR, and electrical analysis of pure and NiO:Li films are studied systematically. From the XRD investigation, the structure of pure and NiO:Li films are polycrystalline with a cubic structure. The average lattice parameter of the pure NiO and NiO:Li films for (200) plane is found to be 4.185 Å which is very close to the standard value. The average crystallite size of the pure NiO and NiO:Li films for (200) plane is 19.12 nm. The SEM morphology showed that the films are formed well and strongly adherent to the substrate. The grain size of NiO:Li films increases with increase in Li concentration. The FTIR studies of pure NiO and NiO:Li films shows the presence of NiO and the inclusion of NiO:Li phase. The optical absorption values are increases while the band gap values are decreases with increase in Li concentration. The band gaps of the films have been calculated by using optical method and it decreases from 3.94 eV to 3.69 eV. The resistivity decreases from 3.20 $\times10^2$ to 0.56 $\times10^2$ Ω cm when the Li concentration increases from 0 to 8%, while the Hall mobility decreases from 5.75 to 2.76 cm^2V^{-1} s^{-1}. The carrier concentration increases from 3.38 $\times10^{15}$ to 3.98 $\times10^{16}$ cm^{-3}. The widened band gap and low resistivity obtained for NiO:Li thin films make them promising candidate for its application as TCO in optoelectronic devices as well as in solar cells.

References

[1] S. Mani Menaka, G. Umadevi, M. Manickam, Materials Chemistry and Physics 191 (2017) 181-187.
[2] S. Mani Menaka, G. Umadevi, Silicon (2018); https://doi.org/10.1007/s12633-017-9716-9.
[3] J.-K. Kang, and S.W. Rhee, Thin Solid Films 391 (2001) 57-61.
[4] I. Fasaki, A. Koutoulaki, M. Kompitsas, C. Charitidis, Appl. Surf. Sci. 257 (2010) 429-433.
[5] K. Nakaoka, J. Ueyama, and K. Ogura, Journal of Electroanalytical Chemistry 571(2004) 93-99.
[6] D.Y. Jiang, J.M. Qin, X. Wang, S. Gao, Q.C. Liang, and J.X. Zhao, Vacuum 86 (2012) 1083-1086.

[7] B. Sasi, K.G. Gopchandran, P.K. Manoj, P. Koshy, P. PrabhakaraRao, V.K. Vaidyan, Vacuum 68 (2003) 149-154.
[8] Shuxi, C.G. Ribbing, E. Wackelgard, Solar Energy Materials & Solar Cells 84 (2004) 193.
[9] Y.R. Park, K.J. Kim, J.Cryst. Growth 258 (2003) 380-384.
[10] A. Reguig, A. Khelil, L. Cattin, M. Morsli, J.C. Berne′de, Appl. Surf. Sci. 253 (2006) 4330.
[11] I.M. Chan, F.C. Hong, Thin Solid Films 450 (2004) 304.
[12] Y.-M. Lee, C.-H. Lai, Solid-State Electron. 53 (2009) 1116-1125.
[13] J.L. Yang, Y.S. Lai, J.S. Chen, Thin Solid Films 488 (2005) 242.
[14] I. Oja , A. Mere , M. Krunks , R. Nisumaa , C.-H. Solterbeck and M. Es-Souni, Thin Solid Films 515 (2005) 674-677.
[15] J. Chavez-Galan, R. Almanza, Solar Ener. 81 (2007) 13.
[16] A.I. Martinez, D.R. Acosta, Thin Solid Films 483 (2005) 107.
[17] H. Kamel, E.K. Elmaghraby, S.A. Ali and K. Abdel-Hady, Thin Solid FilmsVol. 483 (2005) 330-339.
[18] W. Shin, M. Matsumiysa, N. Izu, and N. Murayama, Sens. Actuators B 93 (2003) 304.
[19] P. Mallick and N.C. Mishra, American Journal of Materials Science 2 (2012) 66-71.
[20] I. Hotovy, J. Huran, P. Siciliano, S. Capone, L. Speiss, V. Rehacek, Sens Actuators B 103 (2004) 300–11.
[21] Y. Makimura, A. Rougier, J.M. Tarascon, Appl Surf Sci. 252 (2006) 4593- 8.
[22] L. D. Kadam and P. S. Patil, Sol. Energy Mater. Sol. Cells 69 (2001) 361.
[23] A. Kuzmin, J. Purans, and A.Rodionov, J. Phys: Condens.Mater. 9 (1997) 6979.
[24] Y.M. Lu, W.S. Hwang, J.S. Yang, H.C. Chuang, Thin Solid Films 420-421 (2002) 54-61.
[25] Patterson AL, Phys. Rev. 56 (1939) 978.
[26] B.D. Cullity, S.R. Stock, Elements of X-ray Diffraction, 3rd ed., Prentice Hall, Upper Saddle River, NJ, 2001.
[27] F. Davar, Z. Fereshteh, M. Salavati-Niasari, Journal of alloys and Compounds 476 (2009) 797-801.
[28] Sheikha S. Ashour, Journal of Saudi Chemical Society 18 (2014) 69-76.
[29] Dr. Adel. H. Omran.Alkhayatt, Al-Qadisyah, Journal for Science 14 (2009) 76.
[30] J.M. Shah, Y.L. Li, T. Gessmann, E.F. Schubert, J. Appl. Phys. 94 (2003) 2627-2631.